Supporting Information

Rosenhek-Goldian et al. 10.1073/pnas.1505609112

SI Materials and Methods

Materials. All solvents used for cleaning the SFB and related glassware were analytical grade, while water used was from a Barnstead NanoPure (total organic carbon < 1 ppb) purification system. OMCTS (Fluka, purum grade, 99% pure) was stored under Argon and above 0.4-nm molecular sieves for 2–4 d and then distilled under vacuum in the presence of pure dry filtered Argon. The middle fraction (boiling point = 175 °C) was collected and injected immediately into the force balance by using a flow of dry filtered Argon. Before each experiment, the SFB chamber was initially flushed with dry filtered Argon for 1 h, and was kept dry with P_2O_5. Before each experiment, the distillation system was cleaned with a strong oxidizing solution (a mixture of 66% H_2SO_4 (Palacid Ltd.) and 33% H_2O_2 (Frutarom Ltd.) solution followed by rinsing and sonications with analytical grade toluene and ethanol (Bio-Laboratory Inc.). Mica used was Grade I (S & J Trading). The glue used was sym-diphenylcarbazide (BDH analytical grade), applied by melting on the lenses before depositing the mica sheets.

SFB Measurements. The detailed experimental procedures used to measure the normal and shear forces between mica surfaces using an SFB, shown schematically in Fig. 6*A*, have been described in detail elsewhere (1), including the stringent cleaning procedures. Briefly, thin (1.5–3 μm) crystallographically smooth mica sheets were half-silvered and glued silver side down to plano-cylindrical lenses (radius = 10 mm), which were mounted in the SFB in a cross-cylindrical configuration (Fig. 6*A*). White light multiple beam interferometry measured the mica surface separation D (to ±0.2–0.3 nm for a manual measurement) and their mean surface radius of curvature R via wavelength and shape of fringes of equal chromatic order (FECO, Fig. 6*B*) observed through an eyepiece or via a CCD camera.

Surface approach and retraction was made via a three-stage system, with the finest resolution provided by a piezoelectric tube (P in Fig. 6*A*), which can also move the top surface laterally parallel to the bottom surface (1). Normal forces $F_n(D)$ and shear forces $F_s(D)$ were measured by monitoring the bending of two orthogonal springs (normal spring K_n, constant = 150 N/m; shear force spring K_s, constant =300 N/m) (Fig. 6*A*). K_n may be rigidly clamped if required, as done for the calibration measurements, Fig. 4; K_n bending was determined from the difference between applied normal motion and the change in D (to ±0.2–0.3 nm for manual measurements), while that of K_s was determined via an air gap capacitor probe (to ±0.2–0.3 nm; Accumeasure ASP-1-ILA; MTI Instruments), whose output was recorded simultaneously with the applied voltage causing lateral motion of the top mica surface via P (1).

All preparations (including preparatory mica cleaving) were carried out in a laminar flow hood to minimize contamination. After the lenses with the mica sheets [downstream melt cut (2)] were mounted in the apparatus, the system was calibrated in air by bringing the lenses into contact. Following this, the OMCTS was added to the SFB bath and kept dry via a P_2O_5 reservoir within the SFB.

Dynamic Force Measurement. Normal force profiles $F_n(D)/R$ were recorded in one of two ways: either manually in the usual way (see above, Fig. 1, *Inset*) or via a dynamic approach by high-frame-rate video capture of the FECO while the surfaces approach under an applied constant speed v_{app} (3). Then, the interference fringes (Fig. 6*B*) of the movie frames were analyzed (see above) to obtain the separation, D, as a function of time. The equilibrium normal force $F_n(D)$ between the surfaces was evaluated using the instantaneous balance of forces through Eq. **S1**,

$$F_n(D) = -K_n(\delta D(t)) \qquad \textbf{[S1]}$$

where K_n is the normal spring constant (150 N/m), and $\delta D(t)$ is the deflection of the spring, given by $\delta D(t) = D_{t=0} - D(t) + v_{app}t$. Inertial and hydrodynamic terms (3) were negligible in the region where the structural forces were measured. The v_{app} was determined from the video recording at large separations where $F_n(D) \approx 0$. In addition, a cubic spline algorithm was applied to the data to filter out the noise.

Signal Processing for the Stick–Slip and for the Control Measurements. The primary signal is either the stick slip signal or, for the calibration measurements (Fig. 4), the applied displacement δD_0 signal, together with the fringe position of each video frame. The stick–slip signal and the movement of the fringe were recorded simultaneously, with a possible synchronization mismatch. The primary signal was obtained at a different sampling rate than the fringe position signal: The samples of the primary signal were 0.5 ms apart (a sampling rate of 2 kHz), whereas the samples of the fringe position signal (taken from the video) were ∼8.4 ms apart (as determined by the video frame rate). To correlate one with the other, their sampling rates need to be matched, which is what was done in the sampling rate convergence stage (namely, the sampling rate of the primary signal is reduced to that of the fringe position signal by interpolation).

The natural signal was obtained, as described in *Materials and Methods*, by taking the derivative of the stick–slip signal. In addition, we carried out some standard preprocessing stages, which included trend removal (basically eliminating drift) and scale normalization: To obtain meaningful thresholds, the scales of the signals must match, so they are both normalized to have unit power (namely, they are scaled such that the sum of the squared values for each is 1). The thresholding (given some threshold value h) is simply the operation of setting the functional signal to 1 whenever the natural signal exceeds h, and setting it to zero elsewhere. The threshold value was determined empirically, so as to obtain a functional signal with the same number of peaks as that observed in the natural signal.

There was a difference in the preprocessing of the primary signal between what was done for the control experiments (with applied δD_0, in Fig. 4) and what was done for the stick–slip experiments described above and in *Materials and Methods*. For the stick–slip measurements, we indeed took the derivative of the signal, but for the control experiments, we did not take the derivative, but rather took the signal itself, only with sampling rate conversion and normalization. Thus, there is no essential difference (in the control experiments of Fig. 4) between Fig. 4*A*, *1* and *2*, except that *2* is a scaled and shifted version of *1*, such that its "nonactive" periods are aligned to zero, and its power is normalized to 1.

Details of the Statistical Hypothesis Test. Let us denote the vector of N samples of the natural signal or functional signal during the operation period as $\mathbf{f} = [f[1]\ f[2]\ \ldots\ f[N]]^T$. Assume for now that the delay between the natural (or functional) signal and its presumed occurrence in the measurement signal is known, and equals, without loss of generality, zero. We denote the measured movement signal during the corresponding observation period as $\mathbf{d} = [d[1]\ d[2]\ \ldots\ d[N]]^T$. Likewise, we denote the

(random) vector of samples of the noise signal contaminating the movement measurements as $\mathbf{v} = [\,v[1]\ \ v[2]\ \ \ldots\ \ v[N]\,]^T$.

The two hypotheses in this case take the form $\mathbf{d} = \mathbf{v}$ for H0 and $\mathbf{d} = a \cdot \mathbf{f} + \mathbf{v}$ for H1, where a is an unknown gain parameter, representing the factor by which $\mathbf{f}$ is presumably multiplied for its occurrence in $\mathbf{d}$ (and directly related to the amplitude of the resulting correlated movements).

We assume that the noise $\mathbf{v}$ is taken from a wide-sense stationary, zero mean white Gaussian process with unit variance. The whiteness and Gaussianity assumptions were confirmed via separate statistical tests applied to "noise-only" measurements of the observed movement process (with no stick–slip). The zero mean and unit variance assumptions are enforced by trend removal and scaling applied to the observed signal $\mathbf{d}$ (the possible presence of $a \cdot \mathbf{f}$ in $\mathbf{d}$ is assumed to have a negligible effect, if any, on this normalization, since $a \cdot \mathbf{f}$ is obviously submerged in $\mathbf{v}$, and hence is much weaker).

Under these assumptions, and when a is known, the optimal detector [the Likelihood Ratio Test (LRT), sometimes also called a "Matched Filter" in this context (4, 5)] is obtained by forming the statistic

$$T(\mathbf{d}) = \mathbf{f}^T \cdot \mathbf{d}$$

(a "detection level") and comparing to a threshold λ, subsequently deciding H0 if $T(\mathbf{d}) < \lambda$ and H1 if $T(\mathbf{d}) > \lambda$. To determine the threshold level λ, we observe that, due to the Gaussianity assumption regarding the noise, under H0, $T(\mathbf{d}) \sim N(0, \mathbf{f}^T \cdot \mathbf{f})$ (i.e., is Normally distributed with zero mean and variance $\sigma^2 = \mathbf{f}^T \cdot \mathbf{f}$), whereas under H1, $T(\mathbf{d}) \sim N(a \cdot \mathbf{f}^T \cdot \mathbf{f}, \mathbf{f}^T \cdot \mathbf{f})$ (i.e., is Normally distributed with mean $\mu = a \cdot \mathbf{f}^T \cdot \mathbf{f}$ and the with same variance $\sigma^2 = \mathbf{f}^T \cdot \mathbf{f}$). For convenience, we prenormalize $\mathbf{f}$ to have unit norm, namely $\mathbf{f}^T \cdot \mathbf{f} = 1$, so that $T(\mathbf{d}) \sim N(0,1)$ for H0 and $T(\mathbf{d}) \sim N(a,1)$ for H1. For any given threshold level λ, the resulting false alarm and misdetection probabilities (respectively, the probabilities of deciding H1 when H0 is true and vice versa) would be given, respectively, by

$$\begin{aligned} P_{FA} &= \Pr\{T(\mathbf{d}) > \lambda | H0\} = Q(\lambda) \\ P_{MD} &= \Pr\{T(\mathbf{d}) < \lambda | H1\} = Q(a - \lambda)\,, \end{aligned}$$

where the function

$$Q(x) = \frac{1}{\sqrt{2\pi}} \int_x^\infty e^{-t^2/2} dt$$

denotes the probability that a Normal standard random variable would take a value larger than x.

However, since the true value of a is unknown, only the false alarm probability P_{FA} can be predetermined for any λ, and to set P_{FA} to a prescribed tolerable value ε (e.g., 0.01 or 0.001 in our experiment), one sets $\lambda = Q^{-1}(\varepsilon)$ [where $Q^{-1}(\cdot)$ denotes the inverse function of $Q(\cdot)$]. The resulting false alarm probability would then remain at ε regardless of the value of a, and therefore this strategy for selecting λ is often called CFAR detection. The resulting misdetection probability would obviously depend on a.

Up until now, we assumed that the timing of the presumed occurrence of the natural or functional signal in the measured movement signal was known (and was assumed to occur with zero delay). Obviously, this is not the case in practice, since the measurements of both signals are not time synchronized, and therefore the detection scheme described above has to be applied separately for each possible delay within a reasonable range. In other words, instead of calculating just one detection level $T(\mathbf{d})$, we need to calculate a vector of such levels,

$$T(\mathbf{d};\tau) = \sum_{n=1}^{N} f[n] d[n-\tau] \quad \text{for } t_0 \le \tau \le t_1,$$

where t_0 and t_1 denote the limits of the reasonable delay values (taken in our experiment to be $t_0 = -1[s]$, $t_1 = 1[s]$ (translated to units of samples). Like before, $T(\mathbf{d};\tau)$ is actually the output of a Matched Filter, this time yielding a time-varying signal (through its dependence on τ).

Detection (a decision in favor of H1) is declared if and only if $T(\mathbf{d};\tau)$ exceeds the threshold λ for any of the tested time delays. Since the time delay is estimated as an inherent part of the decision process, such a test is called a GLRT.

A remaining issue for the case of unknown delay is the determination of the threshold value λ, which slightly differs from the case of known delay described above. The difference in this case is that $T(\mathbf{d};\tau)$ receives several "opportunities" to cross the threshold, many more than the single opportunity that $T(\mathbf{d})$ gets in the case of a known delay. Evidently, more opportunities to cross the threshold give rise to a higher false alarm probability (which means that the threshold needs to be set to a higher level). However, these opportunities are not statistically independent, since the value of $T(\mathbf{d};\tau)$ at any value of τ is correlated with its values at neighboring τ. To rigorously account for this dependence, one has to consider the full joint probability distribution of the vector of detection levels

$$\mathbf{T} = [\,T(\mathbf{d};t_0) \quad \cdots \quad T(\mathbf{d};t_1)\,]^T = \mathbf{F} \cdot \tilde{\mathbf{d}}$$

where $\mathbf{F}$ is a Toepliz matrix containing shifted versions of the signal $\mathbf{f}^T$ as its rows, and $\tilde{\mathbf{d}}$ is a long vector of the measured movement signal, covering the entire range of tested delays (with an additional margin of length N, necessary to account for the full signal at the earliest delay). Obviously, under H0 (and under our model assumptions), $\mathbf{T}$ is Normally distributed with zero mean and covariance $\sigma^2 \cdot \mathbf{F} \cdot \mathbf{F}^T$. The exact false alarm probability for any threshold λ can be obtained by multivariate integration of the associated multivariate Normal distribution over the region in which all elements of $\mathbf{T}$ are smaller than λ (followed by subtraction of the result from 1). However, computing the exact value of λ for a prescribed false alarm probability in this way may be prohibitively computationally intense. Instead, we took the following approximate approach: Since the signal $\mathbf{f}^T$ consists of very short pulses of width $\Delta \approx 25$ ms, the correlation between values of $T(\mathbf{d};\tau)$ corresponding to two time delays more than Δ apart would vanish (in other words, the covariance matrix $\sigma^2 \cdot \mathbf{F} \cdot \mathbf{F}^T$ would be roughly banded diagonal with block-sizes corresponding to Δ (in samples) or so. Being jointly Gaussian, any such two uncorrelated values would also be statistically independent. This means that, effectively, the number of independent opportunities for crossing the threshold within a delay span of $t_1 - t_0$ would be $M = (t_1 - t_0)/\Delta$.

Assuming a small false alarm probability p_1 in each independent opportunity, the total false alarm probability in the segment (given by the complementary probability of no false alarm occurring at neither one of the M opportunities) would be

$$P_{FA} = 1 - (1 - p_1)^M \approx M \cdot p_1,$$

where the approximation assumes that p_1 and M are sufficiently small such that $M \cdot p_1 \ll 1$. This implies that the threshold λ for obtaining a prescribed false alarm probability $P_{FA} = \varepsilon$ should be calculated according to the individual probability $P_{FA} = \varepsilon/M$. In other words, the value of λ should be set to

$$\lambda = Q^{-1}\left(\frac{\varepsilon \cdot \Delta}{t_1 - t_0}\right).$$

1. Klein J, Kumacheva E (1998) Simple liquids confined to molecularly thin layers. I. Confinement-induced liquid to solid phase transitions. *J Chem Phys* 108(16):6996–7009.
2. Perkin S, et al. (2006) Forces between mica surfaces, prepared in different ways, across aqueous and nonaqueous liquids confined to molecularly thin films. *Langmuir* 22(14): 6142–6152.
3. Kampf N, Ben-Yaakov D, Andelman D, Safran SA, Klein J (2009) Direct measurement of sub-Debye-length attraction between oppositely charged surfaces. *Phys Rev Lett* 103(11):118304.
4. Kay SM (1998) *Detection Theory*, Fundamentals of Statistical Signal Processing (Prentice Hall, Upper Saddle River, NJ), Vol 2.
5. Van Trees HL, Bell KL, Tian Z (2013) *Detection, Estimation and Modulation Theory Part 1: Detection, Estimation and Filtering Theory* (Wiley, New York), 2nd Ed.

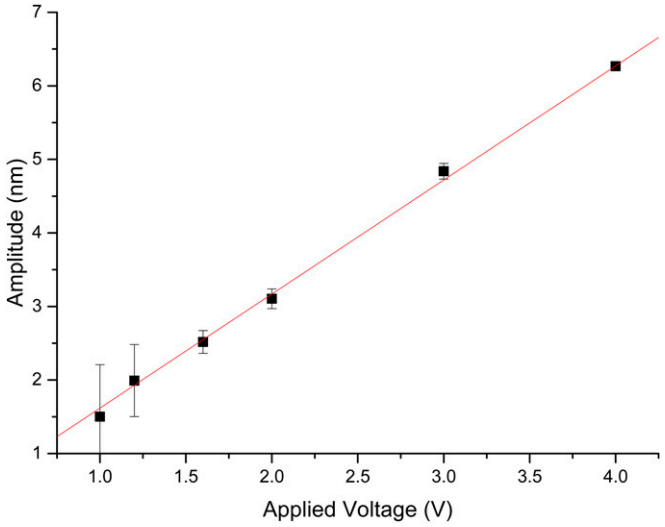

Fig. S1. Calibration graph showing the relation between the applied voltage on the piezo and the actual amplitude of movement (used to generate δD_0 in Fig. 4). Each point represents the average value of 100 measurements. Red line represents the linear fit to the data (slope 1.6 nm/V).

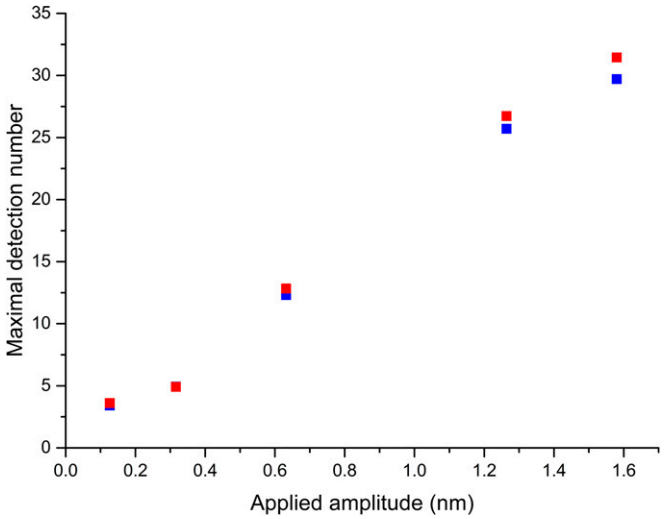

Fig. S2. Calibration graph showing the relation between the applied amplitude δD_0 (as in measurements such as in Fig. 4) of movement and the calculated maximal detection number. Red and blue points are for the natural and functional signals, respectively.